Editors' Suggestion

Temperature-Dependent Photophysics of Single NV Centers in Diamond

Jodok Happacher,[1] Juanita Bocquel,[1] Hossein T. Dinani,[2] Märta A. Tschudin,[1] Patrick Reiser,[1] David A. Broadway,[1] Jeronimo R. Maze,[3] and Patrick Maletinsky[1,*]

[1]*Department of Physics, University of Basel, Klingelbergstrasse 82, Basel CH-4056, Switzerland*
[2]*Escuela de Ingeniería, Facultad de Ciencias, Ingeniería y Tecnología, Universidad Mayor, Santiago 7500994, Chile*
[3]*Facultad de Física, Pontificia Universidad Católica de Chile, Santiago 7820436, Chile*

(Received 26 January 2023; revised 26 April 2023; accepted 14 June 2023; published 24 August 2023)

We present a comprehensive study of the temperature- and magnetic-field-dependent photoluminescence (PL) of individual NV centers in diamond, spanning the temperature-range from cryogenic to ambient conditions. We directly observe the emergence of the NV's room-temperature effective excited-state structure and provide a clear explanation for a previously poorly understood broad quenching of NV PL at intermediate temperatures around 50 K, as well as the subsequent revival of NV PL. We develop a model based on two-phonon orbital averaging that quantitatively explains all of our findings, including the strong impact that strain has on the temperature dependence of the NV's PL. These results complete our understanding of orbital averaging in the NV excited state and have significant implications for the fundamental understanding of the NV center and its applications in quantum sensing.

DOI: 10.1103/PhysRevLett.131.086904

Color centers in solid state hosts are crucial for a variety of quantum technologies, including spin-based quantum sensors [1], highly stable fluorescent labels [2], and single-photon light sources for advanced microscopy [3]. Among the many potential systems, the nitrogen vacancy (NV) lattice defect in diamond stands out due to its multiple demonstrated applications in areas such as nanoscale imaging [4,5] and quantum information processing [6,7], as well as its robustness in a wide range of environmental conditions [8–10], including promising use cases of nanoscale magnetometry in cryogenic conditions [4,5,11].

Most applications of NV centers rely on their highly coherent ground-state electron spin [12] and the ability to efficiently initialize [13,14] and read out [15,16] the spin optically. These techniques are based on a spin-dependent intersystem crossing from the NV's optical excited state to a metastable spin-singlet manifold, from which the system decays into the NV's ground state (GS) [17] [Fig. 1(a)].

This intersystem crossing, and therefore the mechanism of NV spin readout and initialization, results from the properties of the NV's orbital excited states (ESs) and their coupling to the NV's $^1A_1$ singlet state [17]. It is remarkable that, while spin initialization and readout are observed at both cryogenic and ambient conditions, the effective ES level structures are markedly different in the two cases. At temperatures below a few tens of kelvins, and in the limit of sizeable strain, the NV ES exhibits two orbital branches, commonly denoted as E_x and E_y [Fig. 1(a)] [17]. Each of these branches in turn splits into three electronic spin sublevels with magnetic quantum numbers $m_s = -1, 0, +1$. Conversely, at temperatures $T \gtrsim 100$ K, phonon-induced orbital averaging [18] effectively reduces the NV ES to a single orbital with spin 1, where states of magnetic quantum numbers $m_s = \pm 1$ are split from the $m_s = 0$ state by a zero-field splitting of $D_0^{\mathrm{ES}}/h = 1.4$ GHz [Fig. 1(a)] [18–20].

Interestingly, while the foundations of intersystem crossing [35,36] and orbital averaging [18,37,38] have been studied in the past, the transition between the low-temperature and the high-temperature limits, and the emergence of the RT ES spin structure, has never been explored in a systematic way. Prior work on NV ensembles has established a nontrivial temperature dependence of the NV PL intensity at zero magnetic field [37], including a local minimum of the NV PL at $T \approx 40$ K, which remains unexplained thus far. In addition, it was experimentally shown through optical linewidth measurements that orbital averaging between E_x and E_y is dominated by two-phonon mixing processes whose rates scale with temperature as T^5 [18]. So far, however, it remains unexplained how such orbital averaging can account for the nontrivial temperature dependence of the NV's PL intensity, and how the established room-temperature behavior of the NV ES emerges from this picture.

Here, we present a systematic experimental study of the NV photoluminescence (PL) intensity, I_{PL}, as a function of both magnetic field and temperature in the range

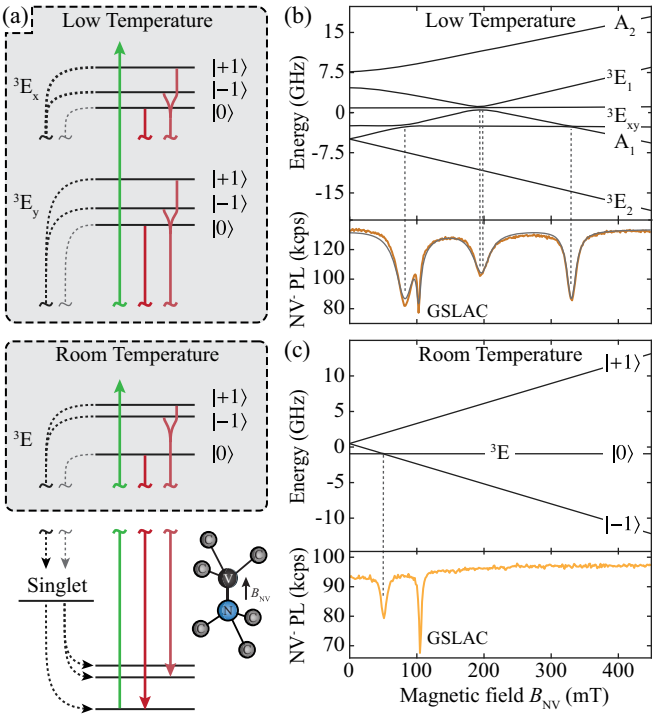

FIG. 1. (a) NV level structure for optical spin pumping and spin readout with the excited-state manifold for both low temperatures (top panel) and the orbital averaged room temperature (middle panel). Additionally, the spin singlet and ground state are also shown, which are applicable for both regimes (bottom panel). (b) The excited-state manifold for an NV spin at $T = 2$ K with relatively low strain $\delta_\perp = 1.685 \pm 0.003$ GHz (top panel) and the corresponding experimental NV PL as a function of applied magnetic field (orange) and fit (gray). (c) Same as in (b), but for $T = 300$ K, for the same low-strain NV. Note that the drop in NV PL occurring at $B_{NV} \approx 100$ mT corresponds to the ground-state level anticrossing (GSLAC).

$T = 2$–300 K, that offers a concise and complete picture of the NV's temperature-dependent photophysics. Our work builds on recent results [39] that revealed key fingerprints of the NV's cryogenic ES level structure through dips in I_{PL} that occur at specific magnetic fields B_{NV} applied along the NV quantization axis. These dips are the result of ES level anticrossings (ESLACs) between levels of unlike m_s that lead to spin mixing and thereby cause an intersystem crossing into the dark singlet states, and therefore a drop in I_{PL}. This process is illustrated by the data presented in Fig. 1(b) that show measurements of I_{PL} as a function of B_{NV} at $T = 2$ K, for an NV with a relatively low strain-induced E_x-E_y level splitting $\delta_\perp \approx 1.6$ GHz [39]. In this work, we exploit this approach to explore the transition of the ES level structure from the cryostat base temperature ($T \approx 2$ K) to ambient ($T \approx 300$ K) and track the emergence of the resulting high-temperature ES level structure [Fig. 1(c)].

Our experiments were performed on two representative, single NV centers that we studied in a variable-temperature, cryogenic confocal microscope (see Ref. [21] for details). The NV centers were located within a few microns of the surface of two ultrapure diamond samples [NV #1: (100)-oriented, electronic grade, Element Six; NV #2: (111)-oriented, custom-grown diamond [40]], and were each embedded in diamond photonic structures to enhance optical collection efficiency [41]. The two NVs differed in the magnitude of the ES strain splitting parameter $\delta_\perp$, which for NV #1 was comparable to ($\delta_\perp = 1.685 \pm 0.003$ GHz)—and for NV #2 much larger than ($\delta_\perp = 75 \pm 2$ GHz)—the NV ES fine-structure splittings, which are $\lesssim 5$ GHz [17]. The quoted strain values were extracted through a model fit to $I_{PL}(B_{NV})$ at $T = 2$ K, as described elsewhere [39]. In all cases, we recorded I_{PL} while sweeping B_{NV} and stepping T under conditions of moderate optical excitation (excitation intensity $\approx 1\times$ optical saturation) with green laser light ($\lambda = 532$ nm).

The experimental data I_{PL} as a function of B_{NV} and T is presented in Figs. 2(a) and 2(c) [42]. A normalization was performed to mitigate the effect of slow fluctuations of I_{PL} over the course of our experiment, which we attribute to drifts in experimental parameters. For the normalization, we first fitted a model [21] [see Eq. (1) and following] to the raw $I_{PL}(T)$ data, as shown in the insets of Figs. 2(a) and 2(c). The fit yields key model parameters [21] and shows qualitatively good agreement with deviations occurring at temperatures where signal drifts were dominant. Second, for each temperature, we used the model prediction for $I_{PL}(B_{NV})$ at our maximal available field $B_{NV} = 800$ mT (where I_{PL} shows the least variation with temperature) to normalize the corresponding dataset $I_{PL}(B_{NV})$.

The resulting, normalized $I_{PL}(B_{NV}, T)$ data for the low-strain NV #1 are shown in Fig. 2(a). At $T = 2$ K, the NV level structure of NV #1 [Fig. 1(b)] results in four sharp I_{PL} dips, which arise from ESLACs occurring both within and between the orbital branches E_x and E_y [39]. With increasing temperature, these ESLAC dips start to broaden, and they reach a maximal width at $T \approx 60$ K, where they span almost the entire magnetic field range accessible in our experiment. Qualitatively, this broadening is well described by the T^5 scaling expected from two-phonon orbital mixing processes [18] [dotted line in Fig. 2(a)].

Remarkably, upon further increasing the temperature, the strongly broadened ESLAC dips disappear, and for $T \approx 70$–150 K, the only discernible feature in $I_{PL}(B_{NV})$ is a narrow dip located at $B_{NV} = 102.4$ mT. This dip results from the NV's well-understood GS level anticrossing (GSLAC) [43,44]. Only at significantly higher temperatures ($T \approx 150$ K) does the single, sharp dip at $B_{NV} = 50.5$ mT appear, which corresponds to the NV's well-known RT ESLAC, appearing in the level structure as illustrated in Fig. 1(c).

We repeated our experiment on the high-strain NV #2 [Fig. 2(c)]. Compared to our findings on NV #1, we find several differences in the evolution of $I_{PL}(B_{NV})$ with

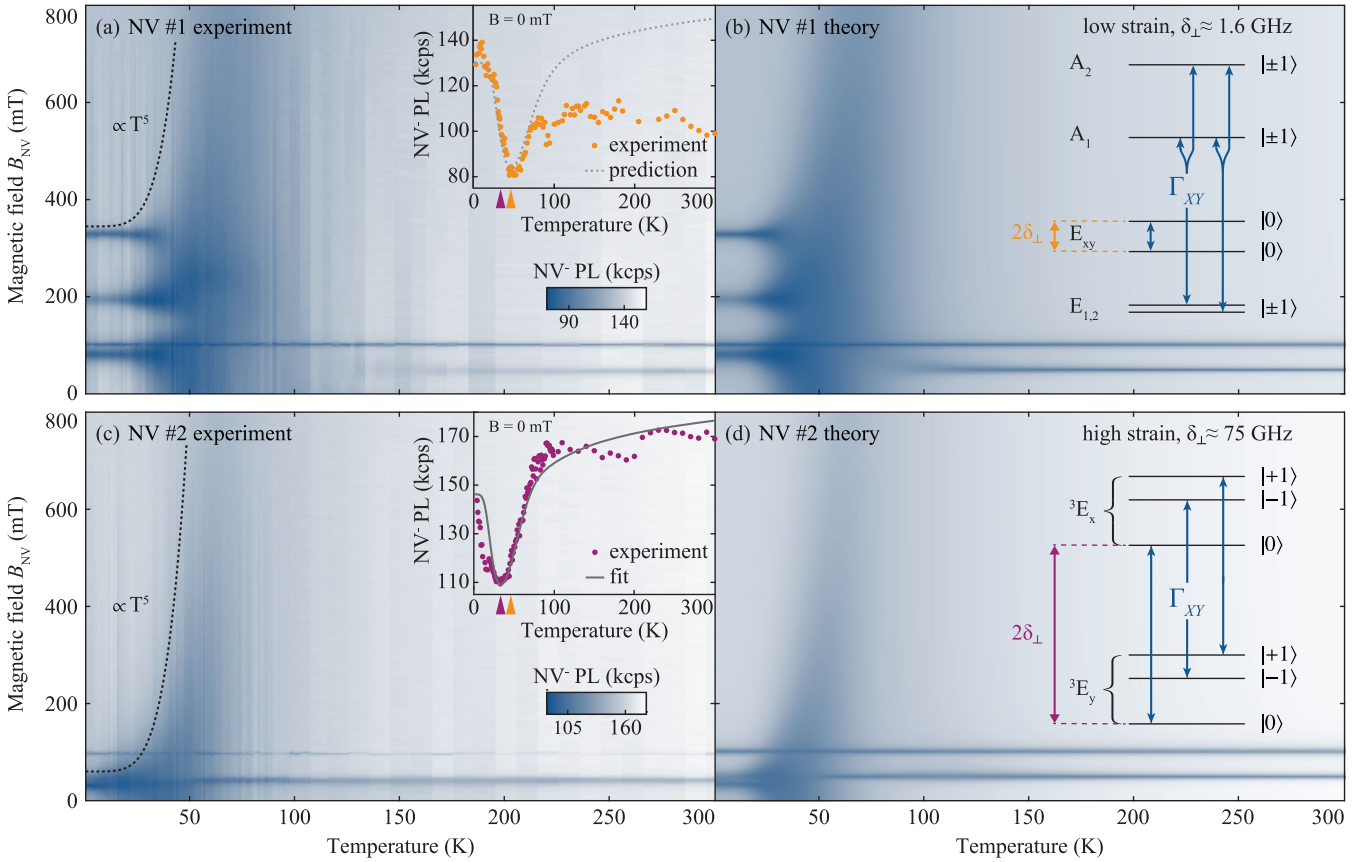

FIG. 2. (a) Experimental data of photoluminescence (PL) intensity I_{PL} recorded on a single NV center with "low" strain (strain parameter $\delta_\perp = 1.685 \pm 0.003$ GHz) as a function of temperature T and magnetic field B_{NV} applied along the NV symmetry axis. I_{PL} data are normalized as described in the text. The dotted line is a guide to the eye for which $B_{\mathrm{NV}} \propto T^5$, scaled to follow the half-width contour of the I_{PL} dip. *Inset:* Raw $I_{\mathrm{PL}}(T)$ data obtained at $B_{\mathrm{NV}} = 0$ mT, together with a model prediction using the extracted phonon coupling from NV #2 data. (b) Model prediction of $I_{\mathrm{PL}}(B_{\mathrm{NV}}, T)$ (see text), with relevant NV excited-state level structure (inset). The rate Γ_{XY} is extracted from fits to NV #2 data, as illustrated in the inset to panel (c). All other NV transition rates are taken from literature [21]. (c) Experimental data as in panel (a), but here taken on a single NV center with "high" strain (strain parameter $\delta_\perp = 75 \pm 2$ GHz). *Inset:* Raw $I_{\mathrm{PL}}(T)$ data obtained at $B_{\mathrm{NV}} = 0$ mT, together with the fit of the model to the raw data. (d) Model prediction, as in panel (b) here, for the "high" strain case. All other rates in the model remain identical. The dip in I_{PL} occurring at $B_{\mathrm{NV}} \approx 100$ mT across all temperatures corresponds to the ground-state level anticrossing (GSLAC).

temperature. At $T = 2$ K, the high-strain NV level structure of NV #2 now results in only two I_{PL} dips, each corresponding to ESLACs occurring within one of the orbital branches [39]. These two ESLAC dips again show a broadening $\propto T^5$ [dotted line in Fig. 2(c)] and merge to a single, broad I_{PL} dip covering the whole accessible range in B_{NV} for $T \approx 50$ K. Upon further increasing the temperature, the strongly broadened ESLAC dips again disappear and, starting from $T \approx 60$ K, are replaced by the RT ESLAC dip discussed before.

To obtain a full understanding of our data, we developed a quantitative model to describe the NV population dynamics as a function of B_{NV} and T that explicitly takes into account the full, low-temperature ES NV level structure [45] and the temperature-dependent, phonon-induced relaxation processes between the involved ESs. For this, we determine the dynamics of the NV's density matrix $\hat{\rho}$ through the Lindblad master equation

$$\frac{d}{dt}\hat{\rho} = \frac{i}{\hbar}[\hat{\rho}, \hat{H}_{\mathrm{NV}}] + \sum_k \hat{L}_k \hat{\rho} \hat{L}_k^\dagger - \frac{1}{2}\{\hat{L}_k^\dagger \hat{L}_k, \hat{\rho}\}, \quad (1)$$

where $\hat{H}_{\mathrm{NV}}$ and $\hat{L}_k$ are the NV Hamiltonian and the relevant collapse operators, respectively. The 10×10 density matrix $\hat{\rho}$ comprises the level structure depicted in Fig. 1(a), specifically the three $^3A_2$ GSs, the six ^3E states, and a single state representing the singlet shelving states $^1A_1$ and E_1. For $\hat{H}_{\mathrm{NV}}$, we employ the well-established NV Hamiltonians for the $^3A_2$ and ^3E manifolds [17,45]. Explicit definitions and expression for $\hat{\rho}$ and $\hat{H}_{\mathrm{NV}}$ are given in Ref. [21].

The collapse operators $\hat{L}_{|i\rangle \to |j\rangle} = \sqrt{\Gamma_{ij}}|j\rangle\langle i|$ describe transitions from states $|i\rangle$ to $|j\rangle$ occurring at rates Γ_{ij}.

The temperature dependence of our I_{PL} data is fully explained by considering the spin-preserving, phonon-induced couplings between the orbital branches E_x and E_y [18] that are described by $\hat{L}_{|X\rangle\to|Y\rangle} = \sqrt{\Gamma_{XY}(T)}|Y\rangle\langle X|$ and its inverse process [46]. Here, $|X\rangle$ ($|Y\rangle$) are state vectors corresponding to the ES E_x (E_y) manifolds. Note that our model fully describes our data by taking into account two-phonon-induced orbital averaging [18], while the previously reported, but weaker one-phonon process [35] has for realistic parameters no observable influence on our model. In addition, we model optical excitation, spontaneous emission, and intersystem crossings with collapse operators between the corresponding orbital manifolds, at rates that we obtain from literature [36,47] and keep constant [48]. We note that temperature dependencies have only been reported for intersystem crossing rates for $T < 20$ K [35], and in this regime have a negligible effect on our findings [39]. In addition, the known temperature-dependent singlet lifetime [49] has been phenomenologically taken into account in our model. The explicit expressions for all collapse operators we employ are given in Ref. [21].

To model the behavior of $I_{\mathrm{PL}}(B_{\mathrm{NV}}, T, \delta_\perp)$, we numerically solve for the steady-state solution of Eq. (1) and determine I_{PL} as being proportional to the total NV ES population for each value of B_{NV} and T [Figs. 2(b) and 2(d)]. The model shows remarkable qualitative and quantitative agreement with our data, both for the high-strain and low-strain cases. The emergence of the RT-ESLAC is quantitatively reproduced in both cases, including the marked difference of the onset temperature for the RT-ESLAC that we discuss below. The simulation uses the magnetic field misalignment to the NV axis measured at low temperature. Some differences between model and data over the entire temperature range can be explained by small variations of this alignment.

Our modeling results offer an intuitive way to understand our experimental findings and the evolution of the ESLAC-induced I_{PL} dips with temperature. At low temperatures, $T \lesssim 10$ K, $I_{\mathrm{PL}}(B_{\mathrm{NV}})$ is unaffected by orbital averaging and only starts to broaden once $\Gamma_{XY} \approx \gamma_{\mathrm{NV}}$, where $\gamma_{\mathrm{NV}} = (12.5\ \mathrm{ns})^{-1}$ is the NV's radiative recombination rate. With increasing temperature, the ES levels—and therefore the ESLACs—start to broaden due to orbital mixing at the rate Γ_{XY}—i.e., $\propto T^5$. The recovery of $I_{\mathrm{PL}}(B_{\mathrm{NV}})$ at $T \gtrsim 60$ K can then be understood as a process akin to motional narrowing in nuclear magnetic resonance [50]: Once Γ_{XY} exceeds $\lambda_{es}^{\perp}$—the rate of spin mixing in the NV's ES [21,39])—jumps between orbital states will interrupt, and therefore effectively suppress ES spin-mixing processes. Since the reduction of I_{PL} results from ESLAC-induced spin mixing and subsequent shelving into the NV singlet states, I_{PL} will recover once $\Gamma_{XY} \gtrsim \lambda_{es}^{\perp}$. After this point in temperature, $I_{\mathrm{PL}}(B_{\mathrm{NV}})$ is governed by the effective RT ES level structure [Fig. 1(c)] and shows the well-known RT-ESLAC. This regime is well described by our model but can alternatively also be derived by taking the partial trace of $\hat{H}_{\mathrm{NV}}$ over the orbital degrees of freedom [21,51].

We note that the quantitative nature of our model also allows us to determine the mixing rate Γ_{XY} induced by the two-phonon process from fits to the data such as the one presented in the inset of Fig. 2(c). In the low-strain case, it yields $\Gamma_{XY} = (1 + \epsilon(T, \delta_\perp)) \cdot \gamma_{\mathrm{NV}} \cdot (0.91 \pm 0.13 \times 10^{-6} K^{-5}) \times T^5$, where ϵ is a weakly temperature- and strain-dependent correction factor, with $\epsilon \ll 1$ for $T \approx 10 \ldots 100$ K [21]. This rate agrees well with prior results [18,35,38], but it was obtained here in a complementary way that does not require complex, resonant laser spectroscopy.

Lastly, we note that our model and data also yield the unexpected observation that the appearance of the RT-ESLAC has a strong strain dependence. The data in Figs. 3(a) and 3(b) illustrate this and show how the RT-ESLAC appears much later for the low-strain NV #1, as compared to the high-strain NV #2. To further support this observation, we

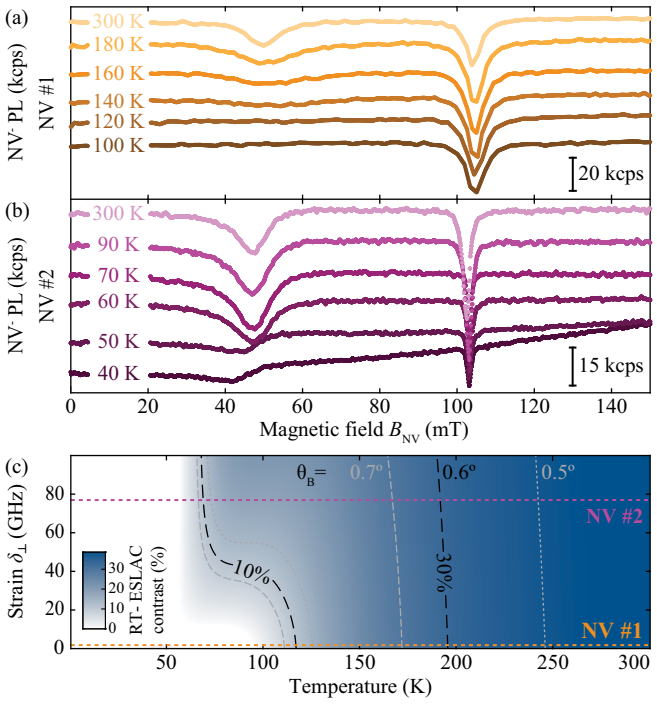

FIG. 3. Appearance of the room-temperature excited-state level anticrossing (RT-ESLAC) for the NVs with (a) low strain and (b) high strain. The data are offset for clarity. For the low-strain NV, the RT-ESLAC appears only at a significantly higher temperature compared to the high-strain NV. (c) Model prediction of the relative change in $I_{\mathrm{PL}}(T, \delta_\perp)$, evaluated at the RT-ESLAC field for a magnetic field misalignment $\theta_B = 0.6°$ (see text and Ref. [21]). Dashed lines mark the position of RT-ESLAC contrast isolines for $\theta_B = 0.6°$ in black, with misalignment increments of $\pm 0.1°$ in gray.

extracted from our model the contribution to I_{PL} originating from the RT-ESLAC alone [21]. We present the resulting model prediction for the relative change in $I_{PL}(T, \delta_\perp)$, evaluated at $B_{NV} = 50.5$ mT—i.e., at the ESLAC field—in Fig. 3(c). The simulation clearly evidences the strong strain dependence as well as the magnetic field misalignment dependence of the onset temperature for the RT-ESLAC, which qualitatively reproduces the experimental data. While the temperature dependence of the ES ODMR for low-strain NVs has been assessed in a prior study [19], its quantitative understanding that we present here has been missing thus far.

In conclusion, we have presented a comprehensive study of the magnetic field and temperature dependence of the PL emission rates of individual NV centers in the limits of both low and high strain. Our work presents a complete picture and a quantitative model of the temperature-induced orbital averaging process that was missing thus far. We demonstrated that two-phonon-induced orbital averaging fully accounts for the previously unexplained NV PL quenching around $T \approx 50$ K and, by virtue of a process akin to motional narrowing, also for the subsequent revival of NV PL for higher temperatures. Our results thereby complement past research on orbital averaging in the NV ES and allow for deeper insight into the orbital averaging and the emergence of an effective room-temperature ES level structure. Next to fundamental insights into the spectroscopic properties of NV centers, our results are of relevance to applications of NV centers in quantum sensing and quantum information processing, in that they predict allowed regions of operation in the parameter space of magnetic field and temperature. Specifically, our experimental data and accompanying theory allow one to identify operational conditions away from ESLACs, where optical spin initialization and readout are most effective.

Importantly, our results have implications beyond pure NV-center-based research. In particular, the methods presented here apply to any color center where ESLACs and spin-dependent dark states (i.e., optically detected spin resonance) occur. Examples for this include SiV centers in SiC [52] or the charge-neutral SiV center in diamond [53], where our method could shed new light into unknown ES structures, orbital averaging, or still poorly understood temperature dependencies in SiV^0 PL [54].

We gratefully acknowledge N. Manson, T. F. Sjolander, and V. Jacques for fruitful discussions, and A. Tallaire and J. Achard for growth of the sample containing NV #2. We further acknowledge financial support from ANID-Fondecyt 1221512 and ANID-Anillo ACT 192023, from NCCR QSIT (Grant No. 185902), from the Swiss Nanoscience Institute, and through Swiss NSF Project Grant No. 188521.

Note added.—Recently, we became aware of related work on NV PL studied at selected temperatures and magnetic fields [55].

*patrick.maletinksy@unibas.ch

[1] C. L. Degen, F. Reinhard, and P. Cappellaro, Rev. Mod. Phys. **89**, 035002 (2017).
[2] M. H. Alkahtani, F. Alghannam, L. Jiang, A. Almethen, A. A. Rampersaud, R. Brick, C. L. Gomes, M. O. Scully, and P. R. Hemmer, Nanophotonics **7**, 1423 (2018).
[3] R. Nelz, M. Radtke, A. Slablab, Z.-Q. Xu, M. Kianinia, C. Li, C. Bradac, I. Aharonovich, and E. Neu, Adv. Quantum Technol. **3**, 1900088 (2020).
[4] L. Thiel, D. Rohner, M. Ganzhorn, P. Appel, E. Neu, B. Müller, R. Kleiner, D. Koelle, and P. Maletinsky, Nat. Nanotechnol. **11**, 677 (2016).
[5] L. Thiel, Z. Wang, M. A. Tschudin, D. Rohner, I. Gutierrez-Lezama, N. Ubrig, M. Gibertini, E. Giannini, A. F. Morpurgo, and P. Maletinsky, Science **364**, 973 (2019).
[6] C. E. Bradley, J. Randall, M. H. Abobeih, R. C. Berrevoets, M. J. Degen, M. A. Bakker, M. Markham, D. J. Twitchen, and T. H. Taminiau, Phys. Rev. X **9**, 031045 (2019).
[7] M. Pompili, S. L. Hermans, S. Baier, H. K. Beukers, P. C. Humphreys, R. N. Schouten, R. F. Vermeulen, M. J. Tiggelman, L. dos Santos Martins, B. Dirkse *et al.*, Science **372**, 259 (2021).
[8] D. M. Toyli, D. J. Christle, A. Alkauskas, B. B. Buckley, C. G. Van de Walle, and D. D. Awschalom, Phys. Rev. X **2**, 031001 (2012).
[9] K.-M. C. Fu, G. Z. Iwata, A. Wickenbrock, and D. Budker, AVS Quantum Sci. **2**, 044702 (2020).
[10] M. Lesik, T. Plisson, L. Toraille, J. Renaud, F. Occelli, M. Schmidt, O. Salord, A. Delobbe, T. Debuisschert, L. Rondin, P. Loubeyre, and J.-F. Roch, Science **366**, 1359 (2019).
[11] M. Pelliccione, A. Jenkins, P. Ovartchaiyapong, C. Reetz, E. Emmanouilidou, N. Ni, and A. C. B. Jayich, Nat. Nanotechnol. **11**, 700 (2016).
[12] G. Balasubramanian, P. Neumann, D. Twitchen, M. Markham, R. Kolesov, N. Mizuochi, J. Isoya, J. Achard, J. Beck, J. Tissler *et al.*, Nat. Mater. **8**, 383 (2009).
[13] J. Harrison, M. J. Sellars, and N. B. Manson, J. Lumin. **107**, 245 (2004).
[14] J.-P. Tetienne, L. Rondin, P. Spinicelli, M. Chipaux, T. Debuisschert, J.-F. Roch, and V. Jacques, New J. Phys. **14**, 103033 (2012).
[15] A. Dréau, M. Lesik, L. Rondin, P. Spinicelli, O. Arcizet, J. F. Roch, and V. Jacques, Phys. Rev. B **84**, 1 (2011).
[16] M. Steiner, P. Neumann, J. Beck, F. Jelezko, and J. Wrachtrup, Phys. Rev. B **81**, 1 (2010).
[17] M. W. Doherty, N. B. Manson, P. Delaney, F. Jelezko, J. Wrachtrup, and L. C. L. Hollenberg, Phys. Rep. **528**, 1 (2013).
[18] K.-M. C. Fu, C. Santori, P. E. Barclay, L. J. Rogers, N. B. Manson, and R. G. Beausoleil, Phys. Rev. Lett. **103** (2009).
[19] A. Batalov, V. Jacques, F. Kaiser, P. Siyushev, P. Neumann, L. J. Rogers, R. L. McMurtrie, N. B. Manson, F. Jelezko, and J. Wrachtrup, Phys. Rev. Lett. **102**, 195506 (2009).

[20] G. D. Fuchs, V. V. Dobrovitski, R. Hanson, A. Batra, C. D. Weis, T. Schenkel, and D. D. Awschalom, Phys. Rev. Lett. **101**, 117601 (2008).

[21] See Supplemental Material at http://link.aps.org/supplemental/10.1103/PhysRevLett.131.086904 for further discussions, which includes Refs. [22–34].

[22] G. Thiering and A. Gali, Phys. Rev. B **98**, 085207 (2018).

[23] Á. Gali, Nanophotonics **8**, 1907 (2019).

[24] V. M. Acosta, A. Jarmola, E. Bauch, and D. Budker, Phys. Rev. B **82**, 201202(R) (2010).

[25] M. C. Cambria, A. Norambuena, H. T. Dinani, G. Thiering, A. Gardill, I. Kemeny, Y. Li, V. Lordi, A. Gali, J. R. Maze, and S. Kolkowitz, Phys. Rev. Lett. **130**, 256903 (2023).

[26] D. Manzano, AIP Adv. **10**, 025106 (2019).

[27] J. Preskill, *Quantum Information and Computation* (California Institution of Technology, Pasadena, 1998).

[28] S. Scopa, G. T. Landi, A. Hammoumi, and D. Karevski, Phys. Rev. A **99**, 022105 (2019).

[29] T. F. Havel, J. Math. Phys. (N.Y.) **44**, 534 (2003).

[30] P. D. Nation, arXiv:1504.06768.

[31] K. J. Brown, E. Chartier, E. M. Sweet, D. A. Hopper, and L. C. Bassett, J. Chem. Health Safety **26**, 40 (2019).

[32] A. Tallaire, J. Achard, A. Boussadi, O. Brinza, A. Gicquel, I. Kupriyanov, Y. Palyanov, G. Sakr, and J. Barjon, Diamond Relat. Mater. **41**, 34 (2014).

[33] M. Lesik, J.-P. Tetienne, A. Tallaire, J. Achard, V. Mille, A. Gicquel, J.-F. Roch, and V. Jacques, Appl. Phys. Lett. **104**, 113107 (2014).

[34] T. A. Abtew, Y. Y. Sun, B.-C. Shih, P. Dev, S. B. Zhang, and P. Zhang, Phys. Rev. Lett. **107**, 146403 (2011).

[35] M. L. Goldman, A. Sipahigil, M. W. Doherty, N. Y. Yao, S. D. Bennett, M. Markham, D. J. Twitchen, N. B. Manson, A. Kubanek, and M. D. Lukin, Phys. Rev. Lett. **114**, 145502 (2015).

[36] M. L. Goldman, M. W. Doherty, A. Sipahigil, N. Y. Yao, S. D. Bennett, N. B. Manson, A. Kubanek, and M. D. Lukin, Phys. Rev. B **91**, 165201 (2015).

[37] L. J. Rogers, R. L. McMurtrie, M. J. Sellars, and N. B. Manson, New J. Phys. **11**, 063007 (2009).

[38] T. Plakhotnik, M. W. Doherty, and N. B. Manson, Phys. Rev. B **92**, 081203(R) (2015).

[39] J. Happacher, D. A. Broadway, J. Bocquel, P. Reiser, A. Jimenéz, M. A. Tschudin, L. Thiel, D. Rohner, M. l. G. Puigibert, B. Shields, J. R. Maze, V. Jacques, and P. Maletinsky, Phys. Rev. Lett. **128**, 177401 (2022).

[40] E. Neu, P. Appel, M. Ganzhorn, J. Miguel-Sánchez, M. Lesik, V. Mille, V. Jacques, A. Tallaire, J. Achard, and P. Maletinsky, Appl. Phys. Lett. **104** (2014).

[41] M. Jamali, I. Gerhardt, M. Rezai, K. Frenner, H. Fedder, and J. Wrachtrup, Rev. Sci. Instrum. **85**, 123703 (2014).

[42] Non-normalized raw data are shown in the Supplemental Material [21] and shows qualitative agreement with the data shown in Figs. 2(a) and 2(c).

[43] D. A. Broadway, J. D. A. Wood, L. T. Hall, A. Stacey, M. Markham, D. A. Simpson, J.-P. Tetienne, and L. C. L. Hollenberg, Phys. Rev. Appl. **6**, 064001 (2016).

[44] A. Wickenbrock, H. Zheng, L. Bougas, N. Leefer, S. Afach, A. Jarmola, V. M. Acosta, and D. Budker, Appl. Phys. Lett. **109**, 053505 (2016).

[45] J. R. Maze, A. Gali, E. Togan, Y. Chu, A. Trifonov, E. Kaxiras, and M. D. Lukin, New J. Phys. **13**, 025025 (2011).

[46] We consider symmetric rates (i.e., $\Gamma_{XY} = \Gamma_{YX}$) only, since the slight asymmetry caused by spontaneous decay $|X\rangle \rightarrow |Y\rangle$ has no measurable effect on our results. The reason for this is that the asymmetry only becomes noticeable once $\Gamma_{XY} \ll \gamma_{\mathrm{NV}}$, in which case the ES dynamics is governed by spontaneous decay into the NV GS.

[47] A. Gupta, L. Hacquebard, and L. Childress, J. Opt. Soc. Am. B **33**, B28 (2016).

[48] We note that our main findings are insensitive to the rates employed, and we find largely identical results by employing other literature values.

[49] L. Robledo, H. Bernien, T. van der Sar, and R. Hanson, New J. Phys. **13**, 025013 (2011).

[50] C. P. Slichter, *Principles of Magnetic Resonance*, Vol. 1 (Springer, Berlin, Heidelberg, 2013).

[51] T. Plakhotnik, M. W. Doherty, J. H. Cole, R. Chapman, and N. B. Manson, Nano Lett. **14**, 4989 (2014).

[52] J.-F. Wang, F.-F. Yan, Q. Li, Z.-H. Liu, H. Liu, G.-P. Guo, L.-P. Guo, X. Zhou, J.-M. Cui, J. Wang, Z.-Q. Zhou, X.-Y. Xu, J.-S. Xu, C.-F. Li, and G.-C. Guo, Phys. Rev. Lett. **124**, 223601 (2020).

[53] B. C. Rose, D. Huang, Z.-H. Zhang, P. Stevenson, A. M. Tyryshkin, S. Sangtawesin, S. Srinivasan, L. Loudin, M. L. Markham, A. M. Edmonds *et al.*, Science **361**, 60 (2018).

[54] U. F. S. D'Haenens-Johansson, A. M. Edmonds, B. L. Green, M. E. Newton, G. Davies, P. M. Martineau, R. U. A. Khan, and D. J. Twitchen, Phys. Rev. B **84**, 245208 (2011).

[55] S. Ernst, P. J. Scheidegger, S. Diesch, L. Lorenzelli, and C. L. Degen, preceding Letter, Phys. Rev. Lett. **131**, 086903 (2023).